



Numerical analysis

Nonlinear artificial viscosity for spectral element methods

*Viscosité artificielle non linéaire pour la méthode des éléments spectraux*Li Lu^a, Murtazo Nazarov^b, Paul Fischer^a^a Urbana, IL, USA^b Uppsala, Sweden

ARTICLE INFO

Article history:

Received 20 November 2018

Accepted 12 July 2019

Available online 23 August 2019

Presented by the Editorial Board

ABSTRACT

We present a filter-based approach to computing artificial viscosities for spectral element methods. A number of applications for this approach are presented.

© 2019 Académie des sciences. Published by Elsevier Masson SAS. All rights reserved.

R É S U M É

Nous présentons une approche basée sur les filtres pour calculer les viscosités artificielles pour la méthode des éléments spectraux. Cette procédure est simple et est mise en œuvre sur un grand nombre d'exemples.

© 2019 Académie des sciences. Published by Elsevier Masson SAS. All rights reserved.

1. Introduction

We develop artificial viscosity schemes for advection-dominated transport problems in the spectral element method (SEM) [11]. With tensor-product Lagrange interpolants based on Gauss–Lobatto–Legendre (GLL) quadrature points, the SEM provides fast and stable operator evaluation along with rapidly (i.e. exponentially) convergent solutions that have minimal numerical dissipation and dispersion for *resolved solution fields*. For marginally resolved fields, such as encountered in large eddy simulation (LES), the SEM suffers dispersion errors typical of all non-dissipative schemes, particularly for the transport of scalars that do not benefit from regularization induced by the pressure/divergence-free constraint imposed on the momentum in the incompressible Navier–Stokes equations. Our goal is to develop robust and practical adaptive dissipation that will control grid-scale oscillations rather than simply advect them with the resolved solution throughout the domain.

Our approach is inspired by earlier work, including the Legendre spectral viscosity (SV) method presented in [5,6], which recovers spectral convergence through post-processing of discontinuous problems. Instead of defining an artificial viscosity, these methods use high-pass filtering on either the numerical solution [6] or the derivatives of the solution [5] to form a Laplace-like viscous regularization. The discontinuity sensor proposed in [12] uses a cut-off high-pass filter on the solution, and is used for evaluating the artificial viscosity for Euler equations. More recently, entropy-based viscosity (EV) methods were introduced in [4], which use a local numerical dissipation that is proportional to an entropy-based error indicator

E-mail addresses: lilu3@illinois.edu (L. Lu), murtazo.nazarov@it.uu.se (M. Nazarov), fischerp@illinois.edu (P. Fischer).

and capped at a maximum of $\nu_h \sim hc/2$, where h is the local grid spacing and c is the local advection speed. This capped viscosity value amounts to the dissipation realized by a stable first-order-upwind discretization in a finite difference setting. We note that similar approaches have been used by other authors, including [8] for the shallow water equations.

2. Formulation

We introduce our formulation using a linear advection problem

$$\frac{\partial \tilde{u}}{\partial t} + \mathbf{c} \cdot \nabla \tilde{u} = 0, \quad \mathbf{x} \in \Omega, t > 0, \tag{1}$$

with appropriate boundary conditions and initial condition $u_0(\mathbf{x})$. We assume throughout this paper that $\nabla \cdot \mathbf{c} = 0$. Equation (1) poses potential difficulties when u_0 has limited regularity. For example, the well-known Gibbs phenomenon shows up if u_0 is a boxcar function. To alleviate this difficulty, we seek artificial viscosity (AV) methods for the SEM. The key idea is to construct an artificial viscosity ν_a and time-march the *modified* governing equation,

$$\frac{\partial \tilde{u}}{\partial t} + \mathbf{c} \cdot \nabla \tilde{u} = \nabla \cdot (\nu_a(\mathbf{x}, t) \nabla \tilde{u}), \quad \mathbf{x} \in \Omega, t > 0. \tag{2}$$

For the SEM, applying a weighted-residual formulation to (2) leads to the system governing the evolution of the basis coefficients, \underline{u} ,

$$B_N \frac{d\underline{u}}{dt} = -C_N \underline{u} - A_N \underline{u}. \tag{3}$$

In one dimension, the respective mass, convective, and stiffness matrices are defined as

$$(B_N)_{ij} = \delta_{ij} \int_{\Omega} \phi_i dx, \quad (C_N)_{ij} = \int_{\Omega} \phi_i c \frac{d\phi_j}{dx} dx, \quad (A_N)_{ij} = \int_{\Omega} \nu_a(x) \frac{d\phi_i}{dx} \frac{d\phi_j}{dx} dx. \tag{4}$$

where the ϕ_i 's are the standard SEM basis functions comprising N th-order Lagrange polynomials based on the Gauss–Lobatto–Legendre (GLL) points in $\hat{\Omega} = [-1, 1]$, which are mapped to each of E elements, Ω^e , $e = 1, \dots, E$. Equation (3) remains unchanged in higher dimensions, save that the definitions (4) are replaced by their d -dimensional counterparts comprising tensor-product Lagrange polynomials in the unit cube, $\hat{\Omega} := [-1, 1]^d$, with isoparametric mappings of $\hat{\Omega}$ to Ω^e for each element. The diagonal (lumped) mass matrix B_N is justified by the use of GLL nodal points (in $\hat{\Omega}$), which yields highly accurate quadrature for the SEM. (Further details are provided in, e.g., [2].)

Ideally, ν_a should be small enough to not compromise accuracy for smooth solutions to (1) but large enough to provide a regularizing effect that improves the behavior of SEM solver in marginally resolved cases. Moreover, we would like solutions to (2) to exhibit monotonicity wherein the extrema of the initial conditions are never exceeded during the course of the calculation. Such a constraint is physical, particularly when (1) is viewed as a model for advection–diffusion, and is important in applications such as combustion, where \tilde{u} would represent concentrations of reactants and products.

A key feature of our approach is that the viscosity ν_a is triggered only by estimated *spatial errors*, meaning that temporal errors, which can be present even when the solution is smooth spatially, will not drive enhanced dissipation. Moreover, ν_a will be present whenever the solution is not smooth in space, even in the limit $\Delta t \rightarrow 0$. Such an approach has the potential to realize enhanced stability while retaining spectral accuracy.

3. Artificial viscosity methods for the SEM

Here, we extend the EV framework in [4] to a form that is suitable for the SEM using a residual/filter-based error indicator. We introduce several stabilization approaches based on variable-viscosity second-order dissipation terms. The methods differ in their choice of error indicators and in details regarding the choice of the capping viscosity and implementation of the artificial dissipation, but they share the common framework that is introduced below.

3.1. Framework

The artificial viscosity method comprises three essential steps: error detection, viscosity bounding, and viscosity regularization. The first step is to define an error indicator $r_E(u)$, and a tentative viscosity,

$$\nu_E(\mathbf{x}) := c_E h^2 r_E(u), \tag{5}$$

where c_E is an order-unity constant. Typically h is the local grid spacing. At gridpoint \mathbf{x}_i , we define as $h_i := (B_N)_{ii}^{-1/d}$, where B_N is the diagonal mass matrix. It is noted in [4] that the precise definition of h has only a weak influence on the method. In the next subsection, we introduce several variants of the error indicator $r_E(u)$, which define different methods.

Second, a viscosity bound is introduced, which for our linear advection equation (1) is

$$\nu_h(\mathbf{x}) := \gamma h |\mathbf{c}|, \tag{6}$$

where $|\mathbf{c}|$ is the local speed, and γ another order-unity constant, usually taken to be 1/2. This viscosity cap is motivated by its correspondence with first-order upwind stabilization. In the finite difference context, this value is sufficiently large to guarantee stability, but sufficiently small to allow explicit time-stepping. (In practical SEM contexts, we use implicit treatment of the viscous terms so the temporal stability issue is not a concern.) The artificial viscosity is set to be the minimum of the computed initial viscosity and the capping viscosity,

$$\nu_a(\mathbf{x}) = \min(\nu_E, \nu_h). \tag{7}$$

Nominally, (7) completes the formulation. However, in the context of the SEM, ν_a can be highly oscillatory. Consequently, some type of regularization is generally employed [4]. We have found that a piecewise-constant viscosity within each element Ω^e usually produces the best solution for SEM. Either the element-wise average of $\nu_a(\mathbf{x})$ or local maximum could be used as the stabilizing viscosity, with the averaging choice less stability-constrained for explicit time-stepping. (An alternative approach based on piecewise-linear Q_1 viscosities within each element yields similar results.)

3.2. Error indicators

In the remainder of this section, we introduce several error indicators. The performance of these indicators is compared in Section 4.

Entropy-based indicators. Following [4], let u be the numerical solution to (1) and let $(E, \mathbf{F}) := (E(u), \mathbf{F}(u))$ be a corresponding entropy pair. For a linear advection equation, an example for such an entropy pair would be $E = u^2/2$, and $\mathbf{F} = \mathbf{c}u^2/2$. The entropy residual is defined as

$$R_E(u) := \frac{\partial E(u)}{\partial t} + \nabla \cdot \mathbf{F}(u), \tag{8}$$

which of course must be approximated numerically. Defining \bar{E} as a representative (globally) space-averaged value of E , we can normalize (8) to obtain the *error indicator function*,

$$r_E(u) := \frac{|R_E(u)|}{\|E(u) - \bar{E}\|_\infty} = \frac{|\frac{\partial E}{\partial t} + \nabla \cdot \mathbf{F}|}{\|E - \bar{E}\|_\infty}. \tag{9}$$

One difficulty with the entropy-based viscosity is that it is not always easy to find well-defined entropy pairs, particularly for more complicated physics. Moreover, an alternative residual-based artificial viscosity method, described in the next section, has been proved to be convergent for finite element solution to conservation laws [9]. Therefore, as an alternative to the entropy-viscosity methods, we seek residual-based error-indicator functions that meet our temporal and spatial requirements. We introduce them as R_1 – R_4 .

Residual-based indicators (R_1). This error indicator derives from the residual in the discretized PDE,

$$R(u) := \left(\frac{\partial u}{\partial t} + \mathbf{c} \cdot \nabla u \right). \tag{10}$$

Unlike the more general entropy-function case, the discretized form of (10) will be identically zero since the solution u^n at time step t^n is in fact defined by setting $R(u^n) = 0$. Consequently, one needs to consider alternative temporal and/or spatial discretizations in order to estimate (10). To advance to time level t^n , one method in [4] evaluates the residual and the relative residual at the preceding timestep as

$$R_1(u) := \left[\frac{\beta_1 u^{n-1} + \beta_2 u^{n-2} + \beta_3 u^{n-3}}{\Delta t} + B_N^{-1} C_N u^{n-1} \right], \quad r_1(u) := \frac{|R_1(u)|}{\|u - \bar{u}\|_\infty}, \tag{11}$$

where β_i represent the second-order backward-difference (BDF2) coefficients. The viscosity-bounding and viscosity-regularization processes (5)–(7) remain unchanged. Higher-order polynomial basis functions are implemented for B_N and C_N in (11) by using a full mass matrix for B_N and exactly integrated advection operator C_N . For a constant velocity advection case, we actually have C_N already exact due to the highly accurate GLL quadrature. The full mass matrix is evaluated by using a M -point GLL quadrature rule where $M \geq N + 1$,

$$(B_N)_{ij}^{\text{full}} = \int_{\Omega} \phi_i \phi_j \, dx. \tag{12}$$

This mass matrix is completely full within each element, resulting in a more expensive inversion, particularly in higher space dimensions $d > 1$. While the assembled matrix is sparse, with $O(EN^{2d})$ nonzeros, we will refer to (12) as the *full mass matrix* in order to distinguish it from its diagonal counterpart, which has only $O(EN^d)$ nonzeros.

It is argued in [4] that the residual-based viscosity (11) is not as robust as the entropy-based viscosity, since the residual will go to zero as the mesh-size goes to zero, whereas the entropy residual converges to a Dirac function found in the shocks. Because of the high-order bases, however, the SEM residual will not vanish in the presence of a shock.

In [4], an example of the temporal difference term in (11) is to use BDF2. When coupled with the underlying $O(h^2)$ finite-element discretization, the residual estimate (11) leads to a viscosity magnitude of $O(h^2\Delta t^2 + h^4)$ when the solution is smooth. The BDF2 variation of definition (11) is suitable only for low order spatial discretization. As remarked in [10], for high-order spatial discretization, higher-order variants of the BDF should be used to avoid significant performance degradations. To remove this dependency on the temporal difference term, in the sequel we introduce error indicators that are based strictly on spatial regularity.

Advection-based residual estimator (R_2). As an alternative to the residual-based viscosity, we replace the temporal difference approximation in (10) with a spatially-driven error indicator. Assuming for simplicity that Euler forward time-stepping is used, the SEM solution to (1) after a single time step would be $\underline{u}^1 = \underline{u}^0 - \Delta t B_N^{-1} C_N \underline{u}^0$. Ideally, if one has access to a solution $\underline{u}_M^1 = \underline{u}^0 - \Delta t \tilde{B}_M^{-1} \tilde{C}_M \underline{u}^0$, where (B_M, C_M) is the mass-convection discretization pair corresponding to some finer resolution than available with the base SEM configuration, then a reasonable error estimate would be $\|\underline{u}_M^1 - \underline{u}^1\|$. If such a solution were available, one would of course take the more accurate \underline{u}_M^1 solution as the output of the time stepper. Thus, it is equally legitimate to consider $M < N$ for the purpose of an estimator, and use the N th-order approximation as the solution. We take $M = N - 1$ and define $\tilde{B}_M = B_N$ and $\tilde{C}_M = J^T C_{N-1} J$, where J is the interpolation routine from the order N SEM mesh to order $N - 1$, while C_{N-1} is the advection operator (3) on the order $N - 1$ mesh. With these matrices, the governing equations for the two resolutions become

$$B_N \frac{du_N}{dt} = -C_N u_N^{n-1}, \quad B_N \frac{d\tilde{u}_N}{dt} = -\tilde{C}_{N-1} u_N^{n-1}. \quad (13)$$

The new error indicator is,

$$R_2(u) := \left[B_N^{-1} (\tilde{C}_{N-1} - C_N) u^{n-1} \right], \quad r_2(u) := \frac{|R_2(u)|}{\|u - \tilde{u}\|_\infty}. \quad (14)$$

The residual (14) plays the same role as (11) in the error indicator in the framework (5). The artificial viscosity method using this error indicator is truly high-order and remains exponentially convergent for smooth problems.

Filtered-advection estimator (R_3). We note that the residual R_2 in (14) is similar to applying C_N to a filtered solution because the advection operators C_N and \tilde{C}_{N-1} differ in their impact on the highest-order modes in the polynomial approximation. This observation suggests the alternative error indicator,

$$R_3(u) := \left[B_N^{-1} C_N \text{HPF}(u^{n-1}) \right], \quad r_3(u) := \frac{|R_3(u)|}{\|u - \tilde{u}\|_\infty}, \quad (15)$$

where $\text{HPF} = I - F$ is a high-pass filter. Here, we take F to be a variant of the local low-pass filter introduced in [7]. Let $L_k(r)$ be the k th-order Legendre polynomial on $\hat{\Omega} := [-1, 1]$, define $\phi_0 = L_0$, $\phi_1 = L_1$, and $\phi_k = L_k - L_{k-2}$ for $k > 1$. These are known as the *bubble functions*. In the reference domain, define the matrix $V_{jk} = \phi_k(\xi_j)$, where $\xi_j \in \hat{\Omega}$ are the GLL nodal points, $j = 0, \dots, N$. The one-dimensional filter is $\hat{F} = V S V^{-1}$, where $S = \text{diag}(\sigma_k)$ constitutes the transfer function in the local modal space. In three dimensions, the filter is $F := \hat{F} \otimes \hat{F} \otimes \hat{F}$, applied to the spectral element nodal coefficients in $\hat{\Omega}$. Typically, we set $\sigma_k = 1$ for low wavenumber modes, $k = 0, \dots, N_c$, and $\sigma_k = 0.5 + 0.5 \times (N - k)/(N - N_c)$ for $k = N_c + 1, \dots, N$. The cut-off wavenumber is usually $N_c \approx 4N/5$. Under this setting, 50% of the energy in the highest mode is eliminated by the low-pass filter. The use of such an aggressive filter is admissible in this context since its role is to trigger an artificial viscosity rather than to modify the solution at each step as a standard filter would do.

For smooth data, $\|\text{HPF}(u)\|$ is exponentially small, implying that $r(u)$ will also be small. In contrast to (14), the advantage of (15) is that it is easy to implement in multiple space dimensions, because it does not require construction of a new advection operator at resolution $N - 1$. For linear problems, the functionality of (15) is clear. If we denote as an error approximation, $e \approx \text{HPF}(u)$, then $r(u)$ is a measure of the amplification of e . Modes that are transparent to HPF and C_N will pass through without amplification. High-wave number modes that are enhanced by C_N will be damped through the action of added dissipation.

We could use a full mass matrix or a diagonal one as B_N for R_2 and R_3 . We compared the results in one-dimensional tests and found that there were no significant improvement in using a full mass matrix for both R_2 and R_3 .

Filter-based gradient estimator (R_4). Finally, we also consider the formula

$$R_4(u) := \left[D_{\text{ref}} h^2 |\nabla \text{HPF}(u^{n-1})|^2 \right], \quad r_4(u) := \frac{R_4}{\|u - \tilde{u}\|_\infty^2}, \quad (16)$$

Table 1
Convergence for $u_0 = \sin \pi x$ at $T = 1$.

N	No AVM	R_1 with BDF2(11)	R_1 with BDF3(11)	R_2 (14)	R_3 (15)	R_4 (16)
4	3.51e-05	5.66e-05	5.36e-05	8.33e-03	3.51e-05	3.51e-05
8	1.03e-10	8.90e-07	4.19e-08	1.82e-08	1.63e-09	1.03e-10
16	5.22e-13	1.69e-08	2.12e-10	8.32e-12	8.32e-12	5.22e-13
32	1.36e-14	3.60e-10	9.30e-13	4.03e-14	4.06e-14	1.36e-14

where D_{ref} is a reference diffusivity that needs to be tuned. This approach differs from (15) in that it does not require application of the advection operator. Consequently, (16) results in dissipation whenever there are sharp gradients, regardless of the advecting field, whereas (15) generates dissipation only by the projection of the scalar gradient onto \mathbf{c} . The advantage of (16) is its relatively low cost and its potential to be applicable in other multi-physics contexts (e.g., the reaction-diffusion equations) where stabilization is required even in the absence of advection.

4. Applications

In this section, we illustrate the effectiveness of the proposed AV methods for a variety of example problems.

Example 1. To begin, we examine the impact of the proposed AV schemes on spectral convergence for a one-dimensional model problem with smooth initial data, $u(x, t = 0) = \sin(\pi x)$, on the periodic domain $\Omega = [0, 1]$. The advection speed is $c = 1$. We use 10 spectral elements of varying order N . Table 1 reports the (pointwise) infinity-norm errors at time $T = 1$ without AVM and with AVM using the four different formulas (R_1 – R_4). RK4 time-stepping is used with the Δt such that the advection CFL based on the minimum grid-spacing is 0.25. The AVM constants used for this problem are $c_E = 1$, $\gamma = 0.5$, and $D_{\text{ref}} = 1$ in (5), (6), and (16), respectively. In (15), the linear low-pass filter uses $N/5$ of the modes (a function of the polynomial order), with a maximum filter strength of $\alpha = 0.5$. We observe that, error indicators R_2 , R_3 and R_4 lead to better accuracy compared to R_1 using either BDF2 or BDF3, since the new schemes do not have a low-order temporal difference term. As expected, R_1 with BDF3 has smaller errors compared to the BDF2 variation.

Full mass matrices are used in evaluating the residual to compute the added viscosity for R_1 – R_3 . R_4 approach does not depend on mass matrices implementation. We compared the results of using full and diagonal mass matrices, which is the usual practice in the SEM, and found that the changes in the error values are not significant. For the time-stepping of the system, only diagonal mass matrices are used.

Example 2. We next consider solutions to the preceding problem with the *nonsmooth* initial data shown in Figs. 1 and 2. The polynomial order is $N = 20$, and the number of elements is $E = 10$ for a total of $n = 200$ points in space. An explicit 4-stage Runge-Kutta method with the Δt such that the CFL based on the minimum grid-spacing is 0.25 is used for time-marching. All AVM constants are identical to those in Example 1.

We are interested in both the short- and long-time behavior. Ideally, the AVM should regularize the non-smooth data in a relatively short time and, thereafter, should weaken to apply minimal local control. At time $T = 1$ (corresponding to one pass through the domain), Fig. 1 shows that, for the given constants, R_1 – R_4 are fairly effective at regularizing the solution. Fig. 2 shows that all methods are effective at time $T = 100$, with R_2 exhibiting more growth in the interface thickness of the boxcar function (center). We remark that the amount of artificial viscosity could be further tuned by adjusting the constant in the capping viscosity. A smaller viscosity would produce higher peak values on the left pulse, but have more oscillations at the top of the boxcar function.

Full mass matrices are used in producing these results. We compared results with using diagonal mass matrices and found that for R_1 the full mass matrices yielded more effective regularization; for R_2 , R_3 the changes in the solution profile are not significant. Therefore, we conducted the following applications in higher dimensions using diagonal mass matrices with R_3 .

Example 3. We turn next to the 2D advection problem for the three-body configuration shown in Figs. 3 and 4. The spectral element code Nek5000 [1] is used in this study. The spatial discretization is based on a 10×10 SEM mesh with periodic boundary conditions and local polynomial order $N = 20$. Time-stepping uses BDF3 for the diffusion terms coupled with 3rd-order extrapolation for advection and a time-step size $\Delta t = 5 \times 10^{-5}$ (CFL = 0.36). The velocity field corresponds to plane rotation such that the initial condition returns to its original position after a single loop at $T = 1$.

Solution fields at time $T = 1$ and $T = 10$ are shown in Figs. 3 and 4. The corresponding minimum and maximum solution values, which should be bounded between 0 and 1, are provided in Table 2. The results indicate that the classical SEM without regularization behaves poorly for this case. (It does not, however, blow-up; the SEM operator is skew-symmetric for this case, with or without de-aliasing [7].) Use of the linear low-pass filter ([3], [7]) significantly reduces the noise in the results, as seen in the center panels of Figs. 3 and 4. Under- and over-shoots, however, are still approximately 20% at both time points $T = 1$ and $T = 10$. The right panels show the AVM results based on R_3 (15). The AVM solution field is visually significantly better and closer to the solution, with much smaller over- and under-shoot values, as evidenced

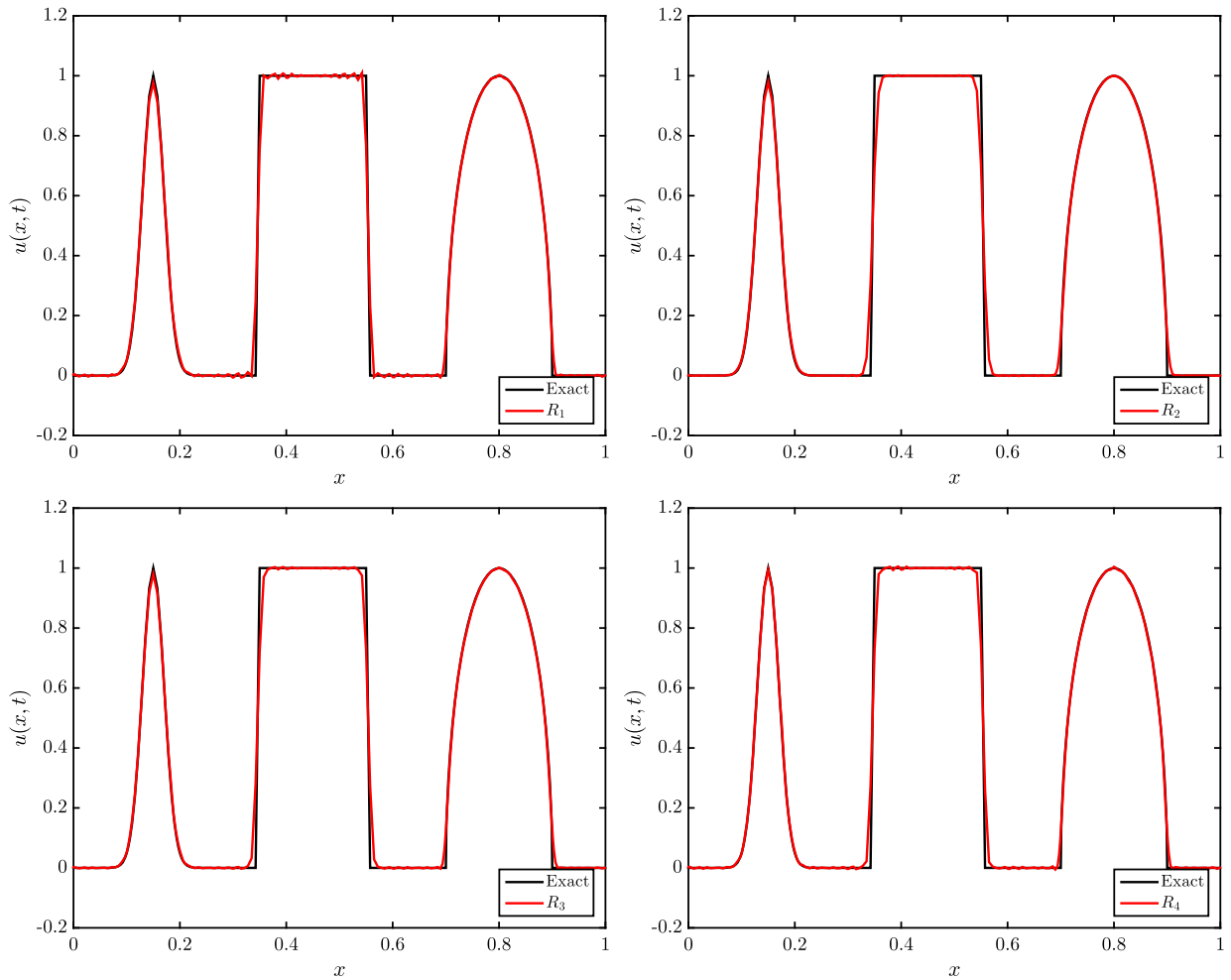


Fig. 1. Solutions to linear advection of non-smooth data, using various AVM, $T = 1$.

by the min and max solution data listed in Table 2. The solutions from the unregularized and filtered approaches are not significantly different between times $T = 1$ and 10. With the AVM, the slot width has grown from diffusion, but the solution has otherwise retained its original form quite well.

For this problem, the constants used in the low-pass filter approach are the highest 2 modes, with a filter strength of $\alpha = 0.05$. For the AVM, the constants used for this problem are $c_E = 0.5$, $\gamma = 0.5$ in (5) and (6). For the constants in the error indicator (15), the linear low-pass filter uses $(N + 1) - \text{int}(3(N + 1)/4)$ modes (6 modes due to the Fortran int function takes the floor integer), with a filter strength of $\alpha = 0.5$.

Example 4. In our final example, we consider an under-resolved scalar advection problem where the velocity field develops from the incompressible Navier–Stokes equations. The flow problem is the double shear layer roll-up problem studied in [3] and elsewhere. In this example, we add an advection-diffusion equation for a scalar field initialized to be the same as the x -velocity component, $T(\mathbf{x}, 0) = u_x(\mathbf{x}, 0)$. A base diffusivity of $\mu = 10^{-5}$ is set in the scalar equation. This case is interesting because the solution ultimately develops shear layers that are thinner than any fixed-resolution grid. The challenge is to control the behavior when this grid-resolution limit is reached.

Once again, we have a doubly-periodic domain on a 10×10 spectral element mesh. The polynomial order for the SEM is $N = 9$ and the solution is advanced with BDF/EXT3 using $\Delta t = 10^{-3}$ (CFL = 0.26). A low-pass filtering strategy using Legendre polynomials is applied to the incompressible Navier–Stokes equations to ensure stability (2 highest modes with filter strength $\alpha = 5\%$). Advection for the velocity and passive scalars are treated with full $3N/2$ de-aliasing (see [7]). Fig. 5 shows the solution at time $T = 2$ for each of three different regularization strategies for the scalar fields along with the min and max solution values at this time. The regularization treatments are: (left) no regularization, (center) low-pass filtering, (right) AVM with R_3 (15). While the results are somewhat subjective, it is arguable that the low-pass filtering delivers the

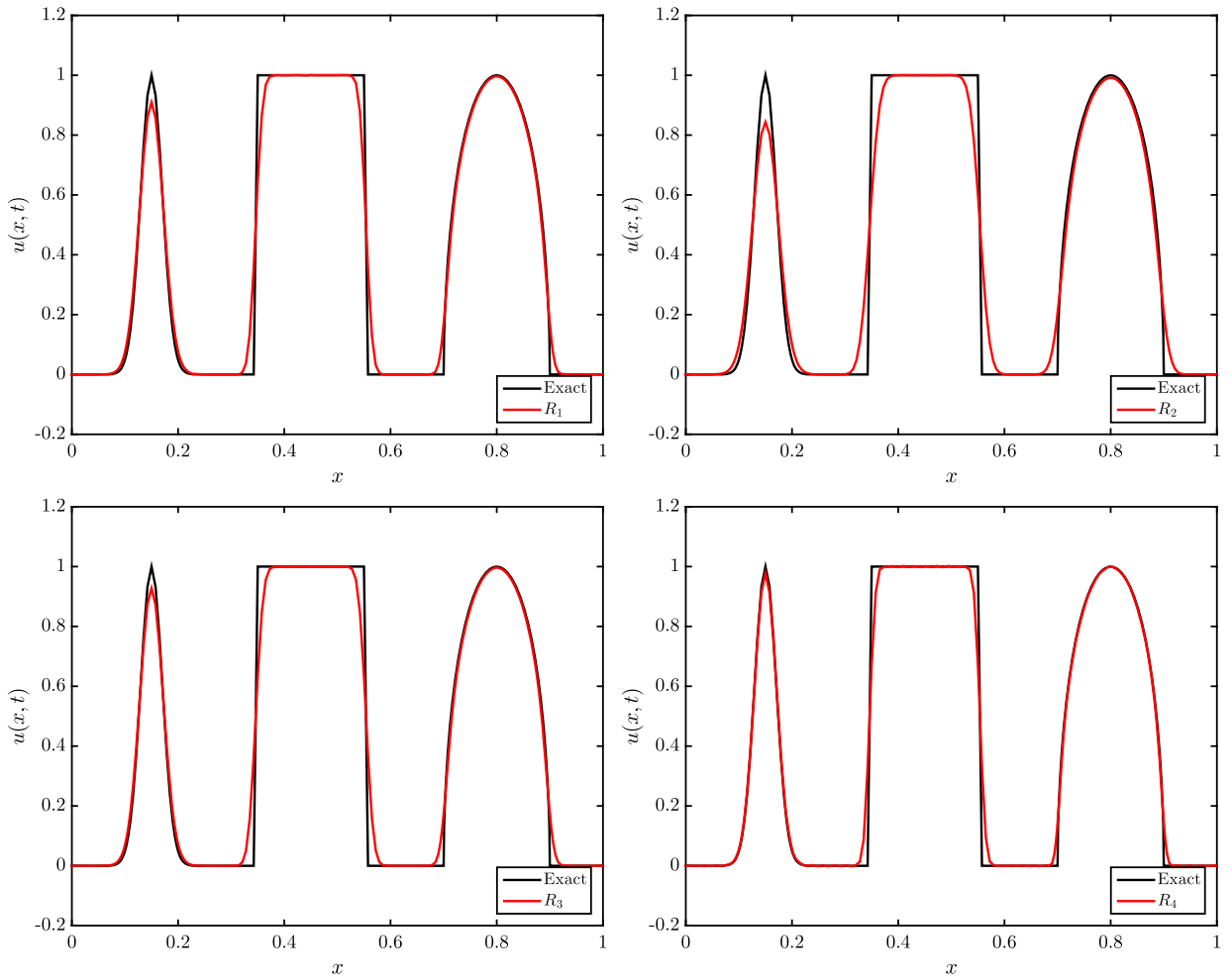


Fig. 2. Same as Fig. 1, at a later time $T = 100$.

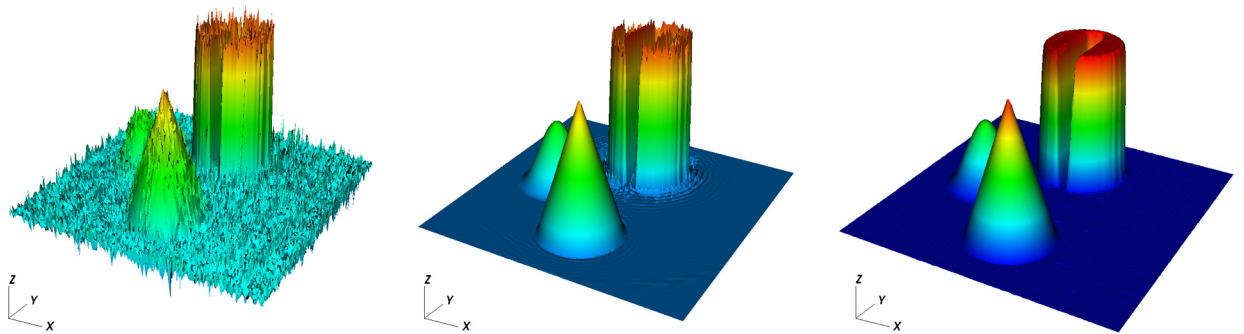


Fig. 3. Solutions at $T = 1$ for the three-body rotation with no filtering (left), with filtering (no viscosity) (center), and with AVM (right).

sharpest result, albeit at the cost of significant under- and over-shoot. The AVM results are more diffused, but the min and max values are within 5% of the expected range.

For the AVM, the constants used are $c_E = 3$ in (5), $\gamma = 0.5$ in (6). The linear low-pass filter for (15) uses $N/5$ of the modes (2 modes), with a filter strength $\alpha = 1$.

The effects of the parameters c_E and α are tabulated below in Table 3.

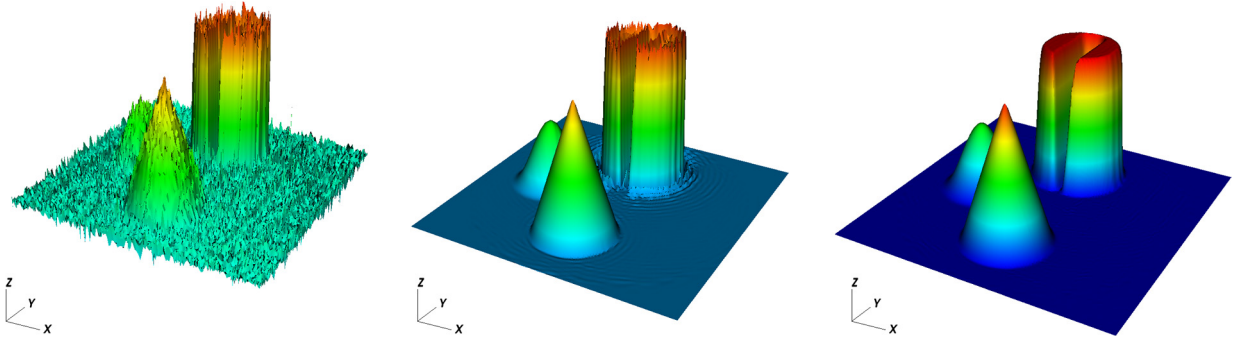


Fig. 4. Solutions at $T = 10$ for the three-body rotation with no filtering (left), with filtering (no viscosity) (center), and with AVM (right).

Table 2
Min and max values for the three-body rotation problem, theoretical $u_{\min} = 0$, $u_{\max} = 1$.

Method	Min at $T = 1$	Max at $T = 1$	Min at $T = 10$	Max at $T = 10$
No filtering	-4.25e-01	1.27e+00	-5.33e-01	1.26e+00
Filtering	-2.03e-01	1.21e+00	-2.32e-01	1.19e+00
AVM	-9.02e-03	1.01e+00	-1.81e-03	1.00e+00

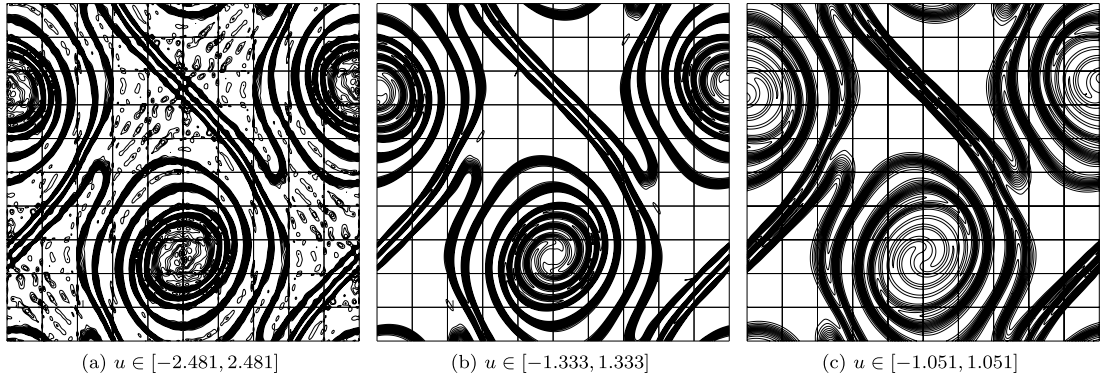


Fig. 5. Solutions at time $T = 2$ for inviscid advection (left), with low-pass filtering (center), and with AVM (right), contours from -1 to 1 by $2/15$.

Table 3
Max overshoots for the double-shear roll-up problem at $T = 2$ using different AVM parameters.

c_E in Eq. (5)	0.5	0.5	1	1	2	3	3
γ in Eq. (6)	0.5	1	0.5	1	0.5	1	0.5
Max overshoot	25%	21%	20%	13%	13%	7%	8%

5. Conclusion

We have investigated several regularization strategies for SEM-based convective transport simulations. The new methods maintain the high-order accuracy of SEM yet provide significant control on under- and overshoots when the solution lacks regularity, which is a feature that is essential for many applications such as large-eddy simulations of combustion. Investigations into maximum-principle preserving high-order artificial viscosity methods are ongoing.

Acknowledgements

This work was supported by the U.S. Department of Energy, Office of Science, the Office of Advanced Scientific Computing Research, under Contract DE-AC02-06CH11357. An award of computer time on Blue Waters was provided by the National Center for Supercomputing Applications. Blue Waters is a sustained-petascale HPC and is a joint effort of the University of Illinois at Urbana-Champaign and its National Center for Supercomputing Applications. The Blue Waters sustained-petascale computing project is supported by the National Science Foundation (awards OCI-0725070 and ACI-1238993) and the state of Illinois. This research used resources of the Argonne Leadership Computing Facility, which is a DOE Office of Science User Facility. The authors would also like to thank Dr. Stefan Kerkemeier for helpful discussions.

References

- [1] Argonne National Laboratory, IL, USA, Nek5000.
- [2] M. Deville, P. Fischer, E. Mund, *High-Order Methods for Incompressible Fluid Flow*, Cambridge University Press, Cambridge, UK, 2002.
- [3] P. Fischer, J. Mullen, Filter-based stabilization of spectral element methods, *C. R. Acad. Sci. Paris, Ser. I* 332 (3) (2001) 265–270.
- [4] J. Guermond, R. Pasquetti, B. Popov, Entropy viscosity method for nonlinear conservation laws, *J. Comput. Phys.* 230 (11) (2011) 4248–4267.
- [5] B. Guo, H. Ma, E. Tadmor, Spectral vanishing viscosity method for nonlinear conservation laws, *SIAM J. Numer. Anal.* 39 (4) (2001) 1254–1268.
- [6] Y. Maday, S. Kaber, E. Tadmor, Legendre pseudospectral viscosity method for nonlinear conservation laws, *SIAM J. Numer. Anal.* 30 (2) (1993) 321–342.
- [7] J. Malm, P. Schlatter, P. Fischer, D. Henningson, Stabilization of the spectral element method in convection dominated flows by recovery of skew-symmetry, *J. Sci. Comput.* 57 (2) (2013) 254–277.
- [8] S. Marras, M. Kopera, E. Constantinescu, J. Suckale, F. Giraldo, A continuous/discontinuous Galerkin solution of the shallow water equations with dynamic viscosity, high-order wetting and drying, and implicit time integration, arXiv preprint, arXiv:1607.04547, 2016.
- [9] M. Nazarov, Convergence of a residual based artificial viscosity finite element method, *Comput. Math. Appl.* 65 (4) (2013) 616–626.
- [10] M. Nazarov, A. Larcher, Numerical investigation of a viscous regularization of the Euler equations by entropy viscosity, *Comput. Methods Appl. Mech. Eng.* 317 (2017) 128–152.
- [11] A. Patera, A spectral element method for fluid dynamics: laminar flow in a channel expansion, *J. Comput. Phys.* 54 (3) (1984) 468–488.
- [12] P. Persson, J. Peraire, Sub-cell shock capturing for discontinuous Galerkin methods, in: *Proc. 44th AIAA Aerospace Sciences Meeting and Exhibit*, Reno, NV, USA, 9–12 January, 2006, p. 112.